ACS OMEGA

http://pubs.acs.org/journal/acsodf

Article

Enhanced Antibacterial and Photoluminescence Activities of ZnSe Nanostructures

Prerna Gupta, Rekha Garg Solanki,* Pushpanjali Patel, KM Sujata, Rakesh Kumar, and Abhay Pandit

Cite This: *ACS Omega* 2023, 8, 13670−13679

Read Online

ACCESS | Metrics & More | Article Recommendations

ABSTRACT: Microorganisms create various health issues; semiconductor nanostructures have raised interest because of antimicrobial properties for suppressing microbial growth. Herein, we report the synthesis of ZnSe nanostructures (NSs) using a green coprecipitation method, and the as-synthesized samples were annealed at 100, 150, and 200 °C temperatures. The synthesized samples were analyzed for structural, morphological, optical, and antibacterial properties. The growth of nanorods was confirmed by TEM micrographs and that of nanoparticles by FESEM and TEM micrographs. The cubic zinc blender phase of samples was confirmed by XRD. The high-intensity electron−phonon (e−ph) interactions and LO modes were confirmed by the Raman spectra. The UV−visible absorption spectra predicted the blue shift in optical band gaps of ZnSe NSs from their bulk counterparts. The PL spectra and associated CIE diagram indicated that the as-synthesized and annealed NSs produce blue color. The investigated antimicrobial activity against *Escherichia coli*, *Pseudomonas aeruginosa*, and *Staphylococcus aureus* implies the superior biological activity of the as-synthesized and annealed samples at 200 °C. The annealing enhances photoluminescence and antimicrobial activities of ZnSe NSs. The enhanced luminscence properties of ZnSe NSs make them suitable for preparing more efficient blue LEDs and lasers for medical applications. The as-synthesized and annealed ZnSe NSs are found effective against the growth of microorganisms, and sustaining this tendency for 1 week provides a strong basis for the development of new drugs against bacterial infections for supporting the pharmaceutical industry.

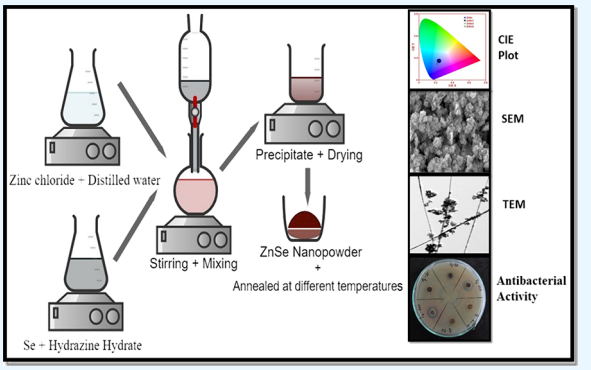

1. INTRODUCTION

Nanotechnology is the most advanced evolving field, with the goal of developing new materials at the nanoscale level.[1,2] Nanotechnology is a major and combined branch of biology, chemistry, physics, medical, and materials science.[3] Semiconductor nanomaterials are an important field of research for not only increasing the efficiency of optoelectronic devices with the synthesis of nanosized materials but also for photocatalytic and antimicrobial applications.[4] The attractive characteristic properties offered by NSs in comparison with their bulk counterparts are as follows: (a) increased ratio of surface to volume, (b) higher optical absorption, (c) low melting point, and (d) quantum tunneling[5] and quantum confinement of charge carriers with confined dimensions as nanoparticles (NPs)/quantum dots (QDs) confined in three dimensions, nanorods (NRs) in two dimensions, and nanofilms (NFMs) in one dimension.[6] Zinc selenide (ZnSe) is a polycrystalline material that occurs in cubic (fcc) and hexagonal (hcp) structures.[7] It is an important semiconductor material of groups II−VI and exhibits a 2.7 eV direct energy band gap for bulk, and its Bohr excitation diameter is 9 nm.[8] The NSs of ZnSe have received a lot of attention because of their unique physical, electrical, chemical, mechanical, catalytic, optical, and antimicrobial properties as compared to the bulk of the same chemical composition.[9,10] It is widely applicable in optoelectronic devices,[11] solar cells,[12] photocatalytic activation,[13] and light-emitting diodes (LEDs),[14] as photoluminescence (PL) material,[15] and in antimicrobial activities.[16]

Bacterial infectious diseases are a global health hazard that affect the economic and societal development. The emergence of stable antibiotic molecules will open new avenues for managing the increased outbreaks of pathogenic and antibiotic-resistant bacterial strains.[17,18] Moreover, novel bacterial mutations and hospital-acquired infections increase the burden of treating such resistant pathogens in underdeveloped countries.[17] Thus, it is highly imperative to discover novel and new antibacterial agents targeting the antibiotic-resistant pathogens that create health havocs in critical obstinate

Received: November 30, 2022
Accepted: March 27, 2023
Published: April 5, 2023

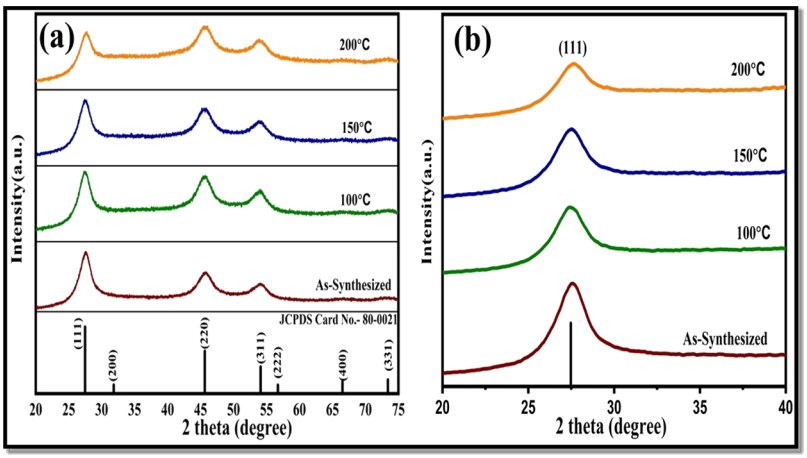

Figure 1. (a) XRD spectra of as-synthesized and annealed ZnSe NSs and (b) enlarged portion of panel (a) in the 2θ range of 20° to 45°.

infections such as *Staphylococcus aureus*, *Pseudomonas aeruginosa*, and *Escherichia coli*.[18] The zinc chalcogenide NSs show antimicrobial activities against the pathogenic agents.[19]

From the past few decades, researchers have put a lot of efforts for the synthesis of ZnSe NSs of desired shape and size. Various physical and chemical methods have been reported for the synthesis of ZnSe NSs such as hydrothermal,[20] sol−gel,[21] reverse micelle,[22] coprecipitation,[23] spray pyrolysis,[24] and chemical bath deposition techniques.[25] The coprecipitation method is one of these techniques that holds great interest because of its simplicity and inexpensiveness.[26]

The present work deals with the synthesis of ZnSe NSs by the coprecipitation method with green growth conditions such as follows: (1) comparative low gowth temperature, (2) DIW used as a solvent, (3) least number of chemicals, (4) no use of organic surfactants, (5) no wastage of chemicals, (6) no release of harmful by-products, (7) low cost, (8) high yield, etc. Hence, the used method is green coprecipitation because of above merits.

Here, we include the synthesis of ZnSe NSs by the green coprecipitation method and observe the infuence of annealing temperature on strutural, morphological, and optical properties. We also observe the applicability of synthesized ZnSe NSs for luminscence and antimicrobial applications. The annealing enhanced the luminscence properties for making more efficient blue LEDs and lasers for medical applications as well as enhanced the suppressing capability against the growth of microorganisms.

2. EXPERIMENTAL PROCEDURE

2.1. Materials. The chemicals used for the synthesis of ZnSe NSs were zinc chloride ($ZnCl_2$) with a minimum assay of 97.0% and hydrazine hydrate ($N_2H_4{\cdot}H_2O$) with a minimum assay of 99.9%; both were purchased from Central Drug House (CDH). Selenium metal powder (Se) with a minimum assay of 99.0% and hydrochloric acid (HCl) with 35% assay were purchased from RANKEM. Ethanol (C_2H_5OH; 99.9%) was purchased from CSS, and deionized water (DIW) was used. All chemicals were utilized in their original and unaltered state after purchase.

2.2. Synthesis of ZnSe NSs. The coprecipitation method with green growth conditions was used for the synthesis of ZnSe NSs. Initially, 2.201 g of zinc chloride ($ZnCl_2$) powder was dissolved in 150 mL of distilled water to obtain its clear solution. In the next step, 3.789 g of selenium powder was dissolved in 20 mL of hydrazine hydrate for obtaining a black solution. Both zinc and selenium solutions were stirred together and heated at 60 °C, maintaining the pH at 10. The stirring and refluxing continue for 8 h. The obtained precipitate (PPT) was separated by centrifugation and washed several times with distilled water and finally with ethanol. The precipitate was dried at 60 °C for 5 h in an open atmosphere, and then a brown-orange-colored powder sample was obtained, which was annealed for 5 h in a vacuum oven at various temperatures, including 100, 150, and 200 °C.

The used method for the synthesis of ZnSe NSs is modified coprecipitation. The used method is ecofriendly in terms of its simplicity, inexpensiveness, and green growth conditions such as comparative low growth temperature, least number of chemicals used, no wastage of chemicals, no use of organic surfactants, DI water used as a solvent, and no release of harmful by-products during synthesis; hence, the used method is safe for the environment and is named as the green coprecipitation method.

2.3. Reaction Mechanism. The reactions of the synthesis process mainly depend on the solvent used and the reaction conditions such as the volume of the solvent, reaction temperature, pH, and surrounding environmental conditions. The possible chemical reactions for the formation of ZnSe NSs are as follows:

$$ZnCl_2 + 2H_2O \rightarrow Zn^{2+} + HCl + 2(OH)^-$$

$$2Se + N_2H_4{\cdot}H_2O \rightarrow (SeN_2H_4{\cdot}H_2O)$$

(intermediate complex and unstable state)

$$2(SeN_2H_4{\cdot}H_2O) \rightarrow 2Se^{2-} + 2\,NH_3 \uparrow + 2OH^-$$

(during synthesis)

$$Zn^{2+} + Se^{2-} \rightarrow ZnSe \downarrow + 2H_2O + N_2 \uparrow + 4H_2O \uparrow$$

(vapors)

2.4. Used Characterization Techniques. The samples were analyzed using XRD, UV−visible, TEM/HRTEM, SEM, EDX, Raman, and PL spectroscopic techniques. A Bruker D8 Advance diffractometer of Cu-Kα radiation (λ = 1.5406 Å) in the range of 10° to 70° with a step size of 0.02° was used to characterize structural properties of the samples. Optical characterization was performed using a Lab India Analytical

https://doi.org/10.1021/acsomega.2c07654
ACS Omega 2023, 8, 13670−13679

Table 1. Structural Parameters of As-Synthesized and Annealed ZnSe NSs at 100, 150, and 200 °C: Peak Positions, Miller Planes (*hkl*), Calculated Crystallite Size, Interplanar Spacing, Microstrain, Dislocation Density, Lattice Parameters, Volume of Unit Cell, etc.

sample code	standard JCPDS card	peak (2θ) for (111)	crystallite size (nm)	lattice constant a (Å)	dislocation density (δ) (nm^{-2})	microstrain ($\varepsilon \times 10^{-3}$)	bond length (Å)	interplanar spacing (Å)	vol. ($Å^3$)
as-synthesized	27.47	27.57	3.80	6.758	68.92	38.18	2.926	3.231	308.737
100 °C	27.47	27.54	3.63	6.766	75.78	40.08	2.929	3.235	309.80
150 °C	27.47	27.58	3.43	6.756	84.65	42.30	2.925	3.231	308.490
200 °C	27.47	27.73	2.68	6.721	138.28	53.78	2.910	3.213	303.613

UV3092 UV−VIS spectrophotometer for synthesized ZnSe NSs dispersed in distilled water. The morphological analysis was carried out using a TEM-TECNAI G2 T30 (S-TWIN) electron microscope and Quanta FEG 250 FESEM with an EDX attachment. Micro-Raman spectroscopy was performed with an excitation wavelength of 532 nm of the xenon laser to obtain phonon vibrational modes of ZnSe NSs. PL measurements were carried out at room temperature with an excitation wavelength of 230 nm.

2.5. Application of ZnSe NSs for Antibacterial Assay. The as-synthesized sample (P1) and sample annealed at 200 °C (P4) of ZnSe NSs were screened for antibacterial activity against *E. coli*, *P. aeruginosa*, and *S. aureus* by the agar well diffusion method described elsewhere[27,28] with minor modifications. Briefly, each bacterial cell was separately cultured in MHB (Mueller Hinton broth) medium overnight at 37 °C, resulting in the primary culture. One hundred microliters of 0.05 OD (optical density) (abs., 600 nm) cells from secondary culture was uniformly spread over the surface of the MHA (Mueller Hinton agar) Petri plate. Three different concentrations (25, 50, and 100 μL) of nanoparticles (50 mg) were spotted in the MHA agar well. The MHA plates with spotted samples were incubated at 37 °C. After 24 h of incubation, the plates were observed for the formation of a zone of inhibition. The observed zone of inhibition was recorded in the cm (centimeter) scale. The retentivity of zones against bacterial growth was also observed for 1 week.

3. RESULTS AND DISCUSSION

3.1. XRD Analysis. The XRD patterns of as-synthesized samples and samples annealed at different temperatures, i.e., 100, 150, and 200 °C, are shown in Figure 1. The XRD patterns were matched and indexed with the standard JCPDS card no. 80-0021 of space group *F*-43*m* of cubic ZnSe. The XRD patterns were indexed on the basis of the intense and prominent peaks corresponding to (111), (220), and (222) reflection planes observed at 27.49°, 45.78°, and 54.04° 2θ values. The XRD patterns show the formation of the pure cubic phase of ZnSe NSs. The annealing process modifies the orientation, shape, and size of crystallites; the resultant is the minor shift observed in peak positions.[29]

Debye Scherrer's formula of eq 1 was used to calculate crystallite size from the full width at half maximum (FWHM) of the intense peak corresponding to (111) reflections of XRD patterns.[30,31]

$$D = \frac{0.9\lambda}{\beta \cos\theta} \tag{1}$$

where D is the crystallite size, λ is the X-ray wavelength (λ = 1.5406 Å), β is the FWHM, and θ is Bragg's angle corresponding to the reflections.

The dislocation density (δ) is the dislocation lines per unit volume of the crystal and is calculated using eq 2.[32]

$$\delta = \frac{n}{D^2} \tag{2}$$

where n equals unity, giving minimum dislocation density.

The microstrain values for (111) reflection peaks are calculated using eq 3 given below as:[33]

$$\varepsilon = \frac{\beta}{4 \tan\theta} \tag{3}$$

where ε is the strain present in the samples, and β is the FWHM.

Bragg's diffraction condition, which is given in eq 4,[34] is used to determine the interplanar spacing "d" corresponding to the (111) reflection plane for all samples as follows:

$$2d \sin\theta = n\lambda \tag{4}$$

where n represents the order of diffraction taken as unity.

The lattice parameter has been calculated for the intense reflection peak for all samples using the formula of eq 5:[35]

$$\frac{1}{d_{hkl}^2} = \frac{a}{\sqrt{h^2 + k^2 + l^2}} \tag{5}$$

The volume of unit cell is calculated using the formula given in eq 6:[36]

$$V = a^3 \tag{6}$$

The bond length of Zn−Se is calculated using the formula for the face-centered cubic structure written in eq 7:[37]

$$2r = \frac{\sqrt{3}a}{4} \tag{7}$$

where "$2r$" is the interatomic separation which is also known as the bond length of Zn−Se.

The calculated values of above parameters are shown in Table 1. We found that the size of the crystallites corresponding to the (111) reflection plane decreases as the annealing temperature increases. Crystallite size changes from 3.8 to 2.7 nm when calculated by Scherrer's formula for as-synthesized samples and samples annealed at 100, 150, and 200 °C. The reason is that the annealing process changes the orientation, shape, and size of crystallites; the resultant is the peak broadening (FWHM) and minor shift in peak positions. The factor peak position and FWHM are incorporated in calculation of the crystallite size by Scherrer's formula. The calculated values of lattice parameters for all samples vary from 6.758 to 6.721 Å. It indicates that with the increase in annealing temperature, the lattice constant decreases. The inverse relation of crystallite size with annealing temperature is

https://doi.org/10.1021/acsomega.2c07654
ACS Omega 2023, 8, 13670−13679

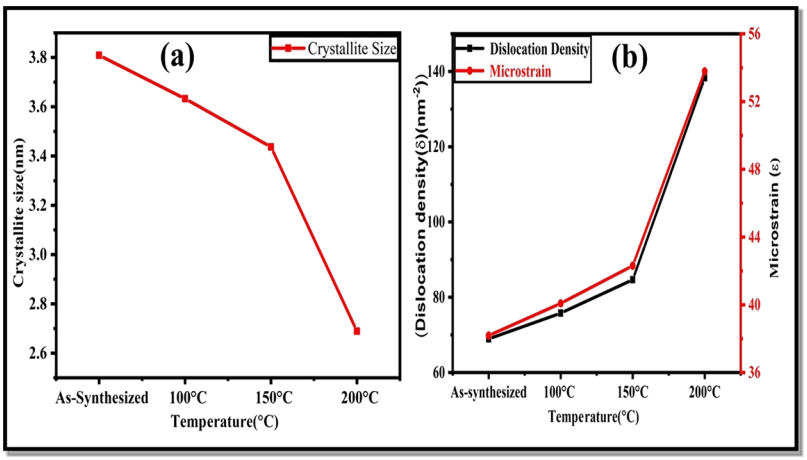

Figure 2. (a) Variation of crystallite size and (b) variation of microstrain and dislocation density with annealing temperature.

also shown in Figure 2a, and the change in microstrain and dislocation density with annealing temperature is shown in Figure 2b.

3.2. TEM, HRTEM, and SAED Analysis. TEM micrographs of as-synthesized and annealed ZnSe NSs are exhibited in Figure 3a–d. The formation of fine and small nanoparticles

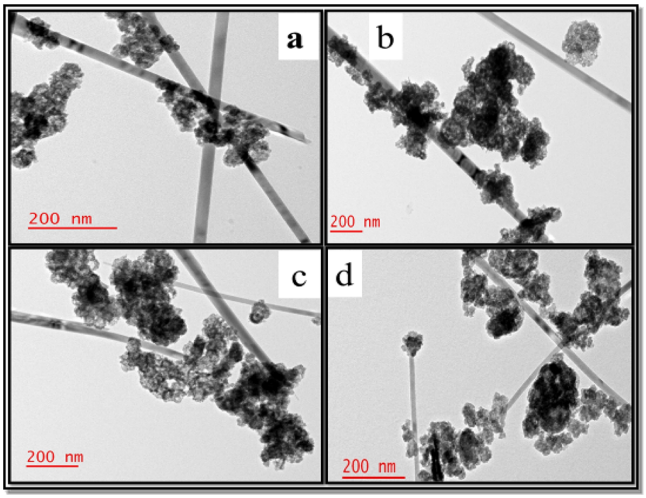

Figure 3. TEM micrographs of ZnSe NSs: (a) as-synthesized and annealed samples (b) at 100 °C, (c) at 150 °C, and (d) at 200 °C.

with nanorods is clearly observed in the micrographs. The nanorods become narrow and fine with an increase in annealing temperature. The length of nanorods varies from 500 to 1050 nm, and the diameter of rods varies from 15 to 70 nm. The agglomeration of nanoparticles also appears in the images, which enhances with the increase in annealing temperature. The crystalline nature of the samples was confirmed by selected area electron diffraction (SAED) patterns, which are shown in Figure 4a–d.

The SAED patterns exhibit a quasi-ring-like diffraction pattern, confirming the formation of the crystalline nature of the ZnSe NSs. The indexation of the rings by (111), (220), and (311) reflection planes is based on the calculated interplanar spacing from the intense rings of SAED patterns (using ImageJ software) and matched the values to the calculated interplanar spacing from corresponding XRD patterns. The dots with fine and intense rings confirm the

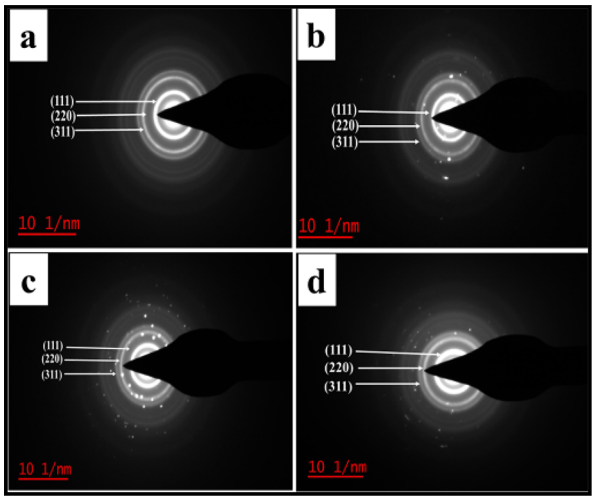

Figure 4. SAED patterns of ZnSe NSs: (a) as-synthesized and annealed samples (b) at 100 °C, (c) at 150 °C, and (d) at 200 °C.

crystallinity of the samples enhanced with annealing temperature. The HRTEM images are shown in Figure 5a–d for as-synthesized and annealed ZnSe NSs, which revealed well-defined lattice planes showing the highly crystalline nature of samples. The estimated interplanar spacing of ZnSe NSs shows variation from d = 0.312 nm to d = 0.330 nm (calculated from ImageJ software). The observed interplanar spacing from the

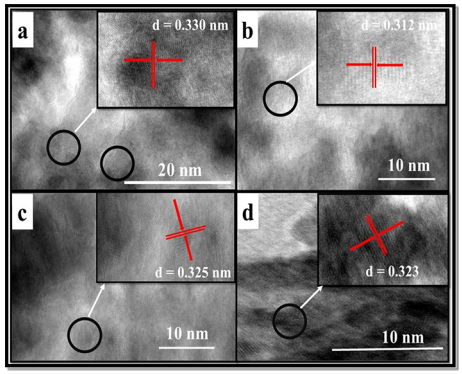

Figure 5. HRTEM micrographs of ZnSe NSs: (a) as-synthesized and annealed samples (b) at 100 °C, (c) at 150 °C, and (d) at 200 °C.

https://doi.org/10.1021/acsomega.2c07654
ACS Omega 2023, 8, 13670−13679

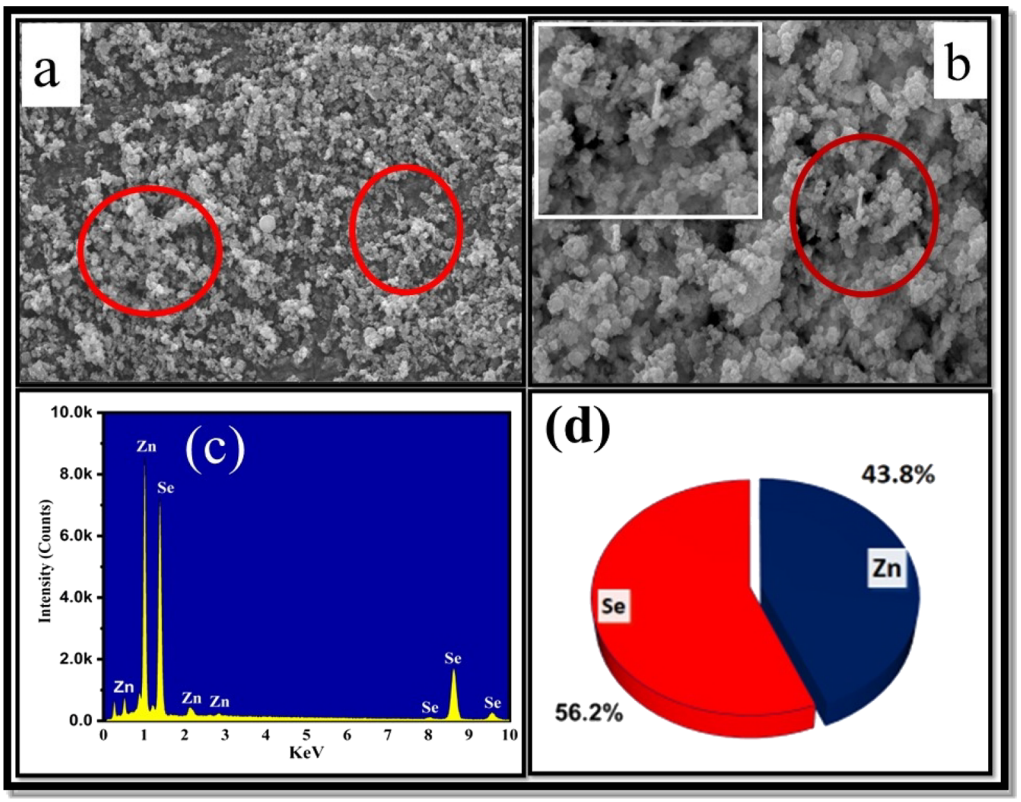

Figure 6. (a) SEM, (b) FESEM micrographs, (c) EDAX spectrum, and (d) compositional pie chart of as-synthesized ZnSe NSs.

HRTEM images is in correlation with the calculated values of interplanar separation corresponding to the XRD diffraction plane of (111) for all samples.

3.3. FESEM Analysis. The FESEM microscopy technique was used to investigate the morphology of as-synthesized ZnSe NSs, and the obtained micrographs are shown in Figure 6a,b. The formation of nanoparticles with nanorods was observed in the FESEM micrograph of the as-synthesized sample. The EDX spectrum of ZnSe NSs is shown in Figure 6c. The EDX spectrum and corresponding compositional results confirm the presence of Zn and Se elements in as-synthesized ZnSe NSs. Figure 6d is a pie chart of the compositional result of ZnSe, which shows the amount of comprising elements in the as-synthesized sample in atomic percentage. The average atomic percentages of zinc and selenium elements are found as 43.8 and 56.2%, respectively. It shows that the as-synthesized sample is little bit zinc-deficient and the zinc deficiency is observed due to the volatile nature of Zn, which diffuses out from the sample during drying. Figure 7a shows the selected area for elemental mapping images of as-synthesized ZnSe NSs. The elemental mapping images are shown in Figure 7b–d. The images clearly show that the constituent elements Zn and Se are homogeneously distributed throughout the sample surface in as-synthesized ZnSe NSs.

3.4. UV–Visible Analysis. The optical properties of as-synthesized and annealed ZnSe NSs were analyzed using UV–visible spectroscopy. The absorption spectra of as-synthesized and annealed ZnSe NSs were recorded in the wavelength range of 350 to 600 nm, and they are shown in Figure 8a–d. The absorption peak for as-synthesized ZnSe NSs is at 431 nm, and those for samples annealed at 100, 150, and 200 °C are obtained at 426, 435, and 438 nm, respectively. The band gap is calculated from the equation $E = hc/\lambda$, where "λ" is the wavelength of the absorption peak, "h" is Planck's constant, and "c" is the speed of light. The obtained band gaps range from 2.87 to 2.74 eV calculated from the peak's wavelength of absorption spectra. It has been found that the band gap decreases as the annealing temperature increases. This may be caused by an increase in particle size. The larger particles are formed by agglomeration of small crystallites as agglomeration is clearly observed in TEM micrographs.

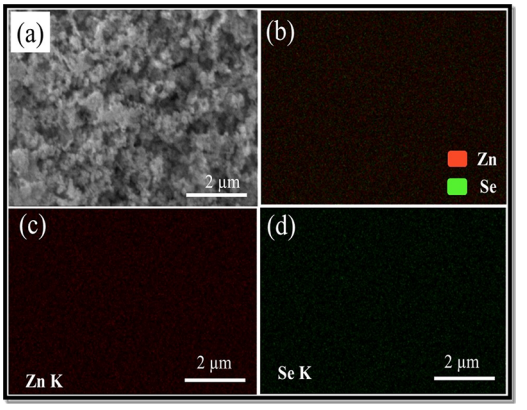

Figure 7. (a) Selected area for elemental mapping and corresponding elemental mapping images of (b) both zinc and selenium, (c) zinc, and (d) selenium.

The particle size of samples was also estimated using the Brus approximation (eq 8) given below as[38−40]

$$E_g(\text{nano}) = E_g(\text{bulk}) + \frac{h^2}{8R^2}\left(\frac{1}{m_e^*} + \frac{1}{m_h^*}\right) - \frac{1.8e^2}{4\pi\varepsilon_0\varepsilon_r R^2} \quad (8)$$

https://doi.org/10.1021/acsomega.2c07654
ACS Omega 2023, 8, 13670−13679

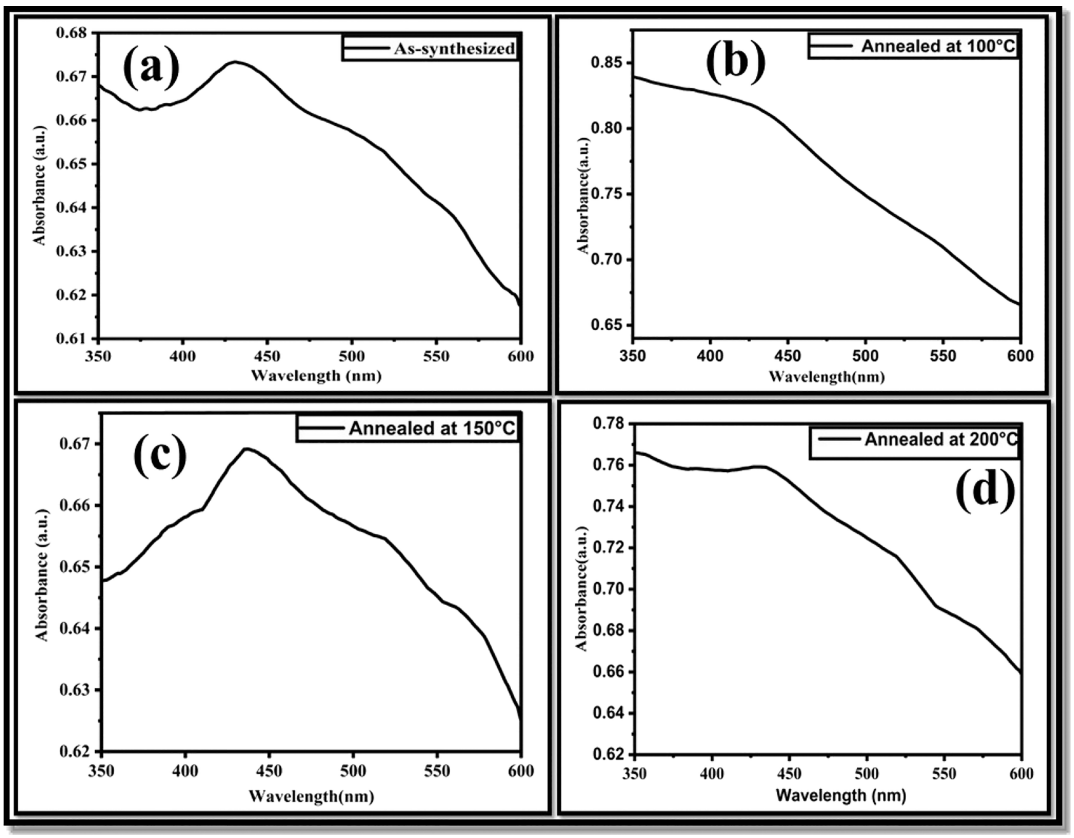

Figure 8. Absorption spectrum of (a) as-synthesized and (b–d) annealed samples.

where E_g (nano) is the band gap energy of nanoparticles, E_g (bulk) is the band gap energy of bulk ZnSe, R is the average radius of particles, m_e* and m_h* are the effective masses of electrons and holes, respectively, and ε stands for the relative dielectric constant (ε = 9.2). The effective masses of electrons and holes are m_e* = 0.17m_o and m_h* = 1.44, where m_o is the free electron mass (9.1×10^{-31} kg). The calculated particle size from the Brus equation for all samples is shown in Table 2.

Table 2. Band Gap and Calculated Particle Size from Brus Approximation and Average Crystallite Size Calculated from XRD Data of All Intense Peaks Using Scherrer's Formula[a]

		crystallite size (nm)	
sample detail	band gap (eV)	calculated from Brus approximation	average crystallite size obtained from all intense peaks of XRD
as-synthesized	2.87	3.14	3.01
100 °C	2.85	3.90	3.51
150 °C	2.83	4.70	4.51
200 °C	2.74	7.81	4.47

[a]Bohr exciton radius, 9 nm.

The particle size is small in comparison to the Bohr exciton radius, showing the quantum confinement effect in as-synthesized and annealed ZnSe NSs. The increase in Brus particle size because of the increased agglomeration of small crystallites via annealing, which is confirmed by the peak broadening observed in XRD and agglomeration observed from TEM micrographs.

3.5. Raman Analysis. The Raman spectra of as-synthesized and annealed ZnSe NSs recorded at room temperature in the range of 100–400 cm^{-1} are shown in Figure 9. The Raman spectra show the two major peaks at 236

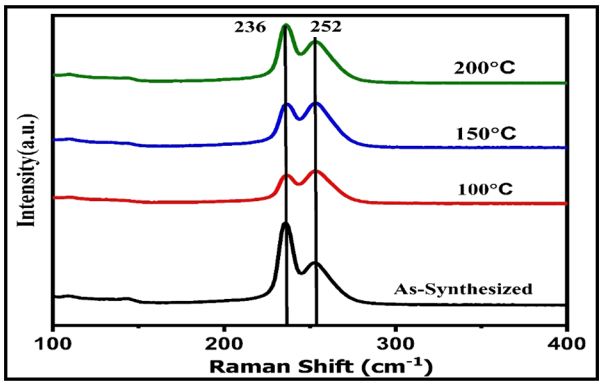

Figure 9. Raman spectra of as-synthesized and annealed samples.

and 252 cm^{-1}.[41] The peak located at 236 cm^{-1} corresponds to the electron–phonon interaction (e–ph),[42] and the peak located at 252 cm^{-1} is the characteristic peak of longitudinal optical (LO) phonon vibrational mode of cubic ZnSe.[43] The as-synthesized sample shows the intense peak at 236 cm^{-1} because of electron–phonon (e–ph) interaction and the peak at 252 cm^{-1} corresponding to the characteristic LO phonon modes of cubic ZnSe. The intensity of electron–phonon interaction mode decreases with the increase in temperature for samples annealed at 100 and 150 °C, and the sample annealed at 200 °C shows an increase in intensity in the similar

https://doi.org/10.1021/acsomega.2c07654
ACS Omega 2023, 8, 13670–13679

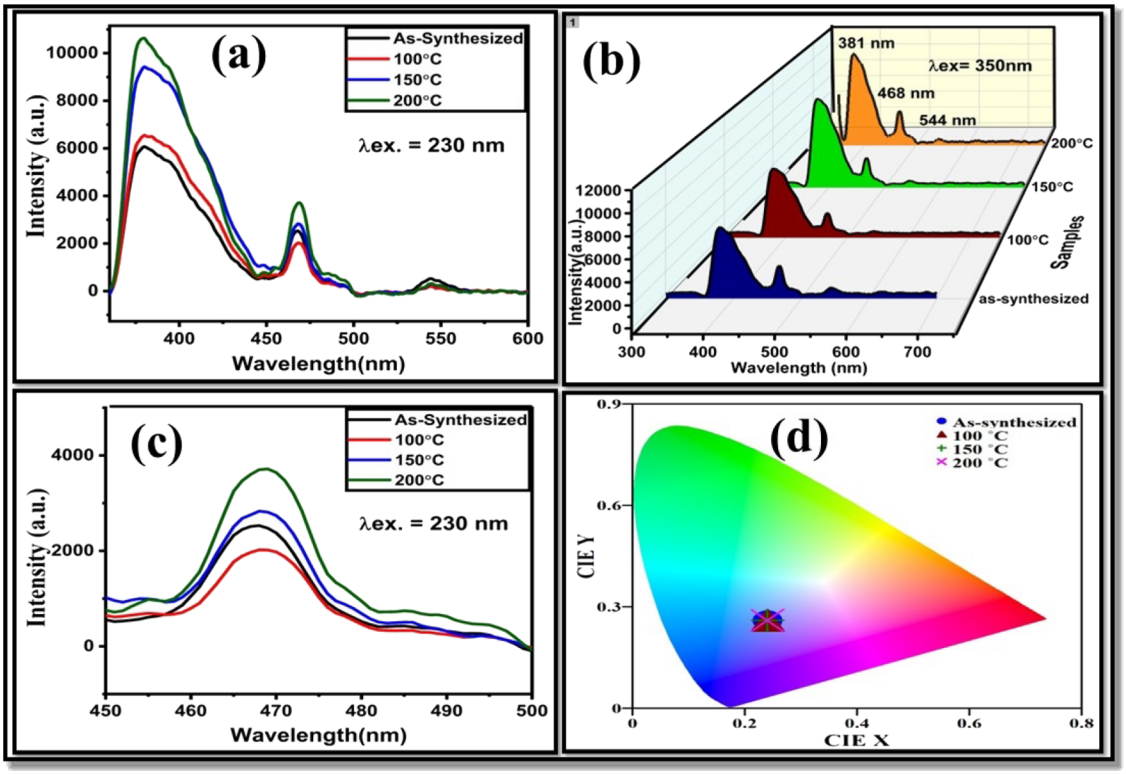

Figure 10. (a) PL spectra, (b) 3D image of PL spectra, (c) enlarged portion of the PL spectra from 450 to 500 nm, and (d) corresponding CIE plots of as-synthesized and annealed samples.

manner to the as-synthesized sample. The e−ph interaction may be less effective for samples annealed at temperatures of 100 and 150 °C, which reduce the intensity and broaden the peak.[41,44] These two samples show that both e−ph modes and LO modes are of equal intensity, while the sample annealed at 200 °C restored the Raman vibrational modes similar to the as-synthesized sample of ZnSe NSs. The Raman modes of phonon vibrations confirmed the formation of the cubic phase of ZnSe, which is in accordance with XRD, HRTEM, and SAED results.

3.6. Photoluminescence Analysis. The photoluminescence spectra are recorded to analyze characteristic emission peaks of the material when excited with high energy than the band gap of the material. The photoluminescence spectra are recorded in the range of 300 to 600 nm. The spectra of the as-prepared and annealed ZnSe NSs are shown in Figure 10a. The samples are excited with 230 nm excitation wavelength. The samples show three emission peaks centered at 381, 468, and 544 nm, and their corresponding energies are 3.25, 2.64, and 2.27 eV, respectively. The PL spectra show the increase in the intensity of emission peaks with the increase in annealing temperature. The strong emission peak centered at around 381 nm (3.25 eV) may be because of the emission of the electron from the band of large energy compared to the band gap of ZnSe NSs, which recombines with the hole of the valence band, i.e., e−hole recombination. The peak observed at 468 nm in the PL spectra of ZnSe NSs is because of the emission that takes place from the bands lying near-band gap edges, i.e., just below the conduction band and just above the valence band, as the band gaps range from 2.74 to 2.87 eV.[45] The peak at 544 nm is because of the transition between impurity bands in ZnSe NSs as the samples are zinc-deficient. The donor bands of selenium and acceptor bands of zinc give impurity transitions (observed in the EDAX spectra).[46] Figure 10b,c shows the 3D surface plot of the PL spectra and the enlarged portion of Figure 10a in the wavelength range of 450 to 500 nm. Both figures clearly indicate the enhanced emission peak intensity. The CIE plot of as-synthesized and annealed ZnSe NSs is shown in Figure 10d. For further investigation of the luminescence properties of as-synthesized and annealed samples, the color coordinates are obtained from the CIE plots. The color coordinates (CCs) and correlated color temperature (CCT) from the emission spectra using CIE diagrams are shown in Table 3. The annealing shifted the color coordinates toward the pure blue region of the CIE diagram and increased the value of CCT, which shows that the annealing increases the tendency of blue emission. Hence, we can say that ZnSe NSs produced a blue color and was found suitable for making blue LEDs and lasers, especially for medical applications.

Table 3. CIE Coordinates and CCT of As-Synthesized and Annealed Samples

sample detail	CIE coordinates (X, Y)	CCT (K)
as-synthesized	X = 0.24, Y = 0.26	20,393
100 °C	X = 0.22, Y = 0.22	81,953
150 °C	X = 0.22, Y = 0.22	81,953
200 °C	X = 0.21, Y = 0.22	95,653

3.7. Antibacterial Activity. The antibacterial activities of P1 (as-synthesized) and P4 (annealed at 200 °C) ZnSe NSs were investigated against *E. coli*, *P. aeruginosa*, and *S. aureus* bacterial species. The formation of the zones of inhibition against these bacterial species shows significant antibacterial activity, thereby restricting the growth. The antibacterial

https://doi.org/10.1021/acsomega.2c07654
ACS Omega 2023, 8, 13670−13679

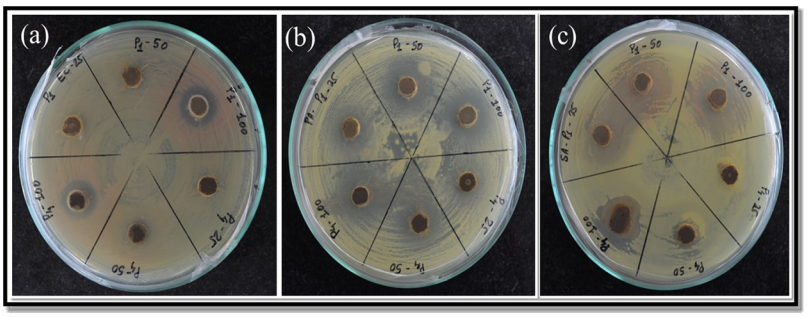

Figure 11. Antibacterial activity of ZnSe NSs (P1 and P4) against (a) *E. coli*, (b) *P. aeruginosa*, and (c) *S. aureus*.

activity of P1 and P4 ZnSe NSs is depicted in Figure 11. In Figure 11a, the antibacterial activity of sample P1 was recorded for 50 μL and higher concentrations against *E. coli* bacteria, while sample P4 shows similar activity at a comparatively low concentration of 25 μL. The antibacterial activity of P1 and P4 against *P. aeruginosa* was observed (Figure 11b) at 25 μL. The same activity was determined against *S. aureus* for P1 and P4 ZnSe NSs; P1 responded at 25 μL and P4 at 50 μL concentration (Figure 11c). Further, the zone of inhibition for these ZnSe NSs has been measured in the cm (centimeter) scale, as represented in Table 4.

Table 4. Measured Zone of Inhibition in the cm (Centimeter) Scale

	zone of inhibition (in cm) against					
	E. coli		*P. aeruginosa*		*S. aureus*	
volume of sample	P1	P4	P1	P4	P1	P4
25 μL	0	0.9	1.3	1.1	0.8	0
50 μL	0.9	1.2	1.9	1.9	1.4	1.2
100 μL	1.6	1.6	2.2	2.3	1.9	2.0

In addition to this, the zone of inhibition was persistent for a period of 1 week. The bar diagram-based representation of antimicrobial activities of samples P1 and P4 against *E. coli*, *P. aeruginosa*, and *S. aureus* bacterial species is shown in Figure 12. P1 (as-synthesized ZnSe NSs) is more effective against the growth of *S. aureus*, and its zone of inhibition increases with the increase in concentration. P4 is effective against all three bacteria, and the zone of inhibition increases with the increase in concentration. Comparative evaluation shows that the zone of inhibition against *P. aeruginosa* is larger than those against *E. coli* and *S. aureus*. On comparison of the behavior of as-synthesized and annealed samples against bacterial growth, we can say that annealing enhances the antimicrobial activity.

4. CONCLUSIONS

ZnSe NSs have been successfully synthesized by a green coprecipitation method and annealed at different temperatures of 100, 150, and 200 °C. XRD results show the formation of a pure cubic zinc blende structure. The crystallite size decreases with the increase in annnealing temperature. TEM micrographs confirmed the formation of concurrent growth of nanoparticles with nanorods, and annealing at different temperatures refined the rod dimensions.The uniform presence of zinc and selenium elements throughout the sample surface was confirmed by the EDX spectra and elemental mapping images. The optical band gap of as-synthesized and annealed samples decreases with the increase in annealing temperature. The as-synthesized and annealed ZnSe NSs show a quantum confinement effect because the average particle size is smaller than the Bohr exciton diameter. The PL spectra and corresponding CIE plot show that all samples are blue color emitters. The sample annealed at 200 °C shows strong blue emission in comparison to other samples, which indicates that annealing enhances the tendency of blue emission. Thus, it can be concluded that the synthesized ZnSe NSs are found suitable for making blue lasers and LEDs, which have applications in the medical field for disease diagnosis and treatment. The sample annealed at 200 °C (P4) is found more effective against

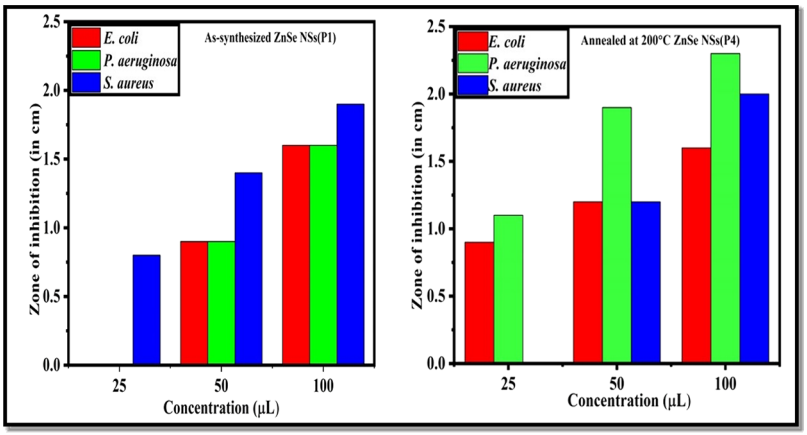

Figure 12. Bar diagram of antibacterial activities for the representing zone of inhibition against *E. coli* (red), *P. aeruginosa* (green), and *S. aureus* (blue).

https://doi.org/10.1021/acsomega.2c07654
ACS Omega 2023, 8, 13670−13679

bacterial growth because of the comparative high tendency of emission of blue color. The antimicrobial activity of ZnSe NSs persisted for 1 week against pathogenic bacteria, providing a strong basis for the development of new drugs against the bacterial infections for supporting the pharmaceutical industry.

AUTHOR INFORMATION

Corresponding Author

Rekha Garg Solanki − *Department of Physics, Dr. Hari Singh Gour University, Sagar, M.P. 470003, India;* orcid.org/0000-0003-3383-8697; Email: rgsolanki@dhsgsu.edu.in, sorekha49@gmail.com

Authors

Prerna Gupta − *Department of Physics, Dr. Hari Singh Gour University, Sagar, M.P. 470003, India*

Pushpanjali Patel − *Department of Physics, Dr. Hari Singh Gour University, Sagar, M.P. 470003, India*

KM Sujata − *Department of Physics, Dr. Hari Singh Gour University, Sagar, M.P. 470003, India*

Rakesh Kumar − *Department of Biotechnology, Central University of South Bihar Gaya, Gaya, Bihar 824236, India*

Abhay Pandit − *Department of Biotechnology, Central University of South Bihar Gaya, Gaya, Bihar 824236, India*

Complete contact information is available at: https://pubs.acs.org/10.1021/acsomega.2c07654

Author Contributions

P.G.: conceptualization, performing experiments and characterization, analysis and interpretation of results, writing of the original draft, and finalization of results and script. P.P.: visualization and support in the formal analysis. K.S.: visualization and support in the formal analysis. R.K.: support in antimicrobial results. A.P.: support in antimicrobial results. R.G.S.: conceptualization, investigation, supervision, project administration, resources, analysis and interpretation of results, editing of the original draft, and finalization of results and script.

Notes

The authors declare no competing financial interest.

ACKNOWLEDGMENTS

The authors would like to thank the Centre for Advanced Research (CAR) Facility of Dr. Hari Singh Gour, Gour University Sagar (M.P.), for XRD results, TEM/HRTEM, and SAED images. The authors would like to thank the Raman spectroscopy facility of Aligarh Muslim University, Aligarh and BITS Pilani Goa, for SEM analysis. The authors are also thankful to the Head, Department of Physics, Head, Department of Chemistry, Dr. Hari Singh Gour University (A Central University), Sagar (M.P.), India, for PL and UV−visible results.

REFERENCES

(1) Fulekar, M. H. Green Synthesis of Zinc Oxide Nanoparticles Using Garlic Skin Extract and Its Characterization. *J. Nanostruct.* **2020**, *10*, 20−27.

(2) Sabir, S.; Arshad, M.; Chaudhari, S. K. Zinc Oxide Nanoparticles for Revolutionizing Agriculture: Synthesis and Applications. *Sci. World J.* **2014**, *2014*, 1.

(3) Ali, M. I.; Sharma, G.; Kumar, M.; Jasuja, N. D. Biological Approach of Zinc Oxide Nanoparticles Synthesis by Cell Free Extract of Spirulina Platensis. *Int. J. Curr. Eng Technol.* **2015**, *5*, 2531−2534.

(4) Suresh, S. Semiconductor Nanomaterials, Methods and Applications: A Review. *Nanosci. Nanotechnol.* **2013**, *3*, 62−74.

(5) Zhang, Q.; Li, H.; Ma, Y.; Zhai, T. ZnSe Nanostructures: Synthesis Properties and Applications. *Prog. Mater. Sci.* **2016**, 472−535.

(6) Asha, A. B.; Narain, R. *Nanomaterials Properties*; Elsevier Inc., 2020. DOI: 10.1016/B978-0-12-816806-6.00015-7.

(7) Senthilkumar, K.; Kalaivani, T.; Kanagesan, S.; Balasubramanian, V.; Balakrishnan, J. Wurtzite ZnSe Quantum Dots: Synthesis, Characterization and PL Properties. *J. Mater. Sci.: Mater. Electron.* **2013**, *24*, 692−696.

(8) Ghosh, K.; Gupta, P.; Pandey, R. K. Optical Properties Tuning by Sodium and Magnesium Co-Doping in ZnO Thin Films for Optoelectronic Applications. *Mater. Today Proc.* **2020**, *28*, 177−181.

(9) Sundrarajan, M.; Ambika, S.; Bharathi, K. Plant-Extract Mediated Synthesis of ZnO Nanoparticles Using Pongamia Pinnata and Their Activity against Pathogenic Bacteria. *Adv. Powder Technol.* **2015**, *26*, 1294−1299.

(10) Zewde, D.; Geremew, B. Biosynthesis of ZnO Nanoparticles Using *Hagenia Abyssinica* Leaf Extracts; Their Photocatalytic and Antibacterial Activities. *Environ. Pollut. Bioavail.* **2022**, *34*, 224−235.

(11) Sharma, J.; Shikha, D.; Tripathi, S. K. Optical and Electrical Properties of ZnSe Thin Films: Effect of Vacuum Annealing. *Rom. Rep. Phys.* **2014**, *66*, 1002−1011.

(12) Okereke, N. A.; Ekpunobi, A. J. ZnSe Buffer Layer Deposition for Solar Cell Application. *J. Non oxide Glasses* **2015**, 31.

(13) Li, X.; Wei, B.; Wang, J.; Li, X.; Zhai, H.; Wang, D.; Liu, Y.; Sui, Y.; Zhang, Q.; Yang, J. Fabrication and Comparison of the Photocatalytic Activity of ZnSe Microflowers and Nanosheets. *J. Mater. Sci.: Mater. Electron.* **2015**, *26*, 8484−8488.

(14) Kadim, A. M. Zinc Selenide Quantum Dots Light Emitting Devices (ZnSe QDs-LEDs) with Different Organic Polymers. *Nano Hybrids Compos.* **2017**, *18*, 11−19.

(15) Colibaba, G. V.; Nedeoglo, D. D. Photoluminescence of the ZnSe Single Crystals Doped by Thermal Diffusion of Nitrogen. *Phys. B* **2009**, *404*, 184−189.

(16) Souri, D.; Salimi, N.; Ghabooli, M. Hydrothermal Fabrication of Pure ZnSe Nanocrystals at Different Microwave Irradiation Times and Their Disc-Diffusion Antibacterial Potential against Gram Negative Bacteria: Bio-Optical Advantages. *Inorg. Chem. Commun.* **2021**, *123*, No. 108345.

(17) Sirelkhatim, A.; Mahmud, S.; Seeni, A.; Kaus, N. H. M.; Ann, L. C.; Bakhori, S. K. M.; Hasan, H.; Mohamad, D. Review on Zinc Oxide Nanoparticles: Antibacterial Activity and Toxicity Mechanism. *Nano-Micro Lett.* **2015**, 219−242.

(18) Darroudi, M.; KhandaKhandan Nasab, N.; Salimizand, H.; Dehnad, A. Green Synthesis and Antibacterial Activity of Zinc Selenide (ZnSe) Nanoparticles. *Nanomed. J.* **2019**, *6*, 258−263.

(19) Navale, G. R.; Late, D. J.; Shinde, S. S. JSM Nanotechnology & Nanomedicine Antimicrobial Activity of ZnO Nanoparticles against Pathogenic Bacteria and Fungi. *JSM Nanotechnol. Nanomed.* **2015**, *3*, 1−9.

(20) Sobhani, A.; Salavati-Niasari, M. Optimized Synthesis of ZnSe Nanocrystals by Hydrothermal Method. *J. Mater. Sci.: Mater. Electron.* **2016**, *27*, 293−303.

(21) Hutagalung, S. D.; Loo, S. C. Zinc Selenide (ZnSe) Nanoparticles Prepared by Sol-Gel Method. *2007 7th IEEE Int Conf Nanotechnol - IEEE-NANO 2007, Proc* 2007, 930−933. DOI: 10.1109/NANO.2007.4601336.

(22) Lei, Z.; Wei, X.; Bi, S.; He, R. Reverse Micelle Synthesis and Characterization of ZnSe Nanoparticles. *Mater. Lett.* **2008**, *62*, 3694−3696.

(23) Ayodhya, D. Synthesis, Characterization of ZnS Nanoparticles by Coprecipitation Method Using Various Capping Agents - Photocatalytic Activity and Kinetic Study. *IOSR J. Appl. Chem.* **2013**, *6*, 01−09.

(24) Kabir, M. H.; Ali, M. M.; Kaiyum, M. A.; Rahman, M. S. Effect of Annealing Temperature on Structural Morphological and Optical

Properties of Spray Pyrolized Al-Doped ZnO Thin Films. *J. Phys. Commun.* **2019**, *3*, 105007.
(25) Lokhande, C. D.; Patil, P. S.; Tributsch, H.; Ennaoui, A. ZnSe Thin Films by Chemical Bath Deposition Method. *Sol. Energy Mater. Sol. Cells* **1998**, *55*, 379−393.
(26) Farahmandjou, M.; Jurablu, S. Co-Precipitation Synthesis of Zinc Oxide (ZnO) Nanoparticles by Zinc Nitrate Precursor. *Int.J. Bio-Inorg. Hybrid Nanomater.* **2014**, *3*, 179−184.
(27) Magaldi, S.; Mata-Essayag, S.; Hartung De Capriles, C.; Perez, C.; Colella, M. T.; Olaizola, C.; Ontiveros, Y. Well Diffusion for Antifungal Susceptibility Testing. *Int. J. Infect Dis.* **2004**, *8*, 39−45.
(28) Kumar, S.; Kumar, A.; Kaushal, M.; Kumar, P.; Mukhopadhyay, K.; Kumar, A. Fungal-Derived Xenobiotic Exhibits Antibacterial and Antibiofilm Activity against *Staphylococcus Aureus*. *Drug Discovery Ther.* **2018**, *12*, 214−223.
(29) Yadav, K.; Dwivedi, Y.; Jaggi, N. Effect of Annealing Temperature on the Structural and Optical Properties of ZnSe Nanoparticles. *J. Mater. Sci.: Mater. Electron.* **2015**, *26*, 2198−2204.
(30) Koshy, J.; George, K. C. Annealing Effects on Crystallite Size and Band Gap of CuO Nanoparticles. *Int. J. Mater. Phys.* **2014**, *5*, 35−42.
(31) Gupta, P.; Patel, P.; Sujata, K. M.; Solanki, R. G. Synthesis and Characterization of ZnSe Nanorods by Coprecipitation Method. *Mater. Today Proc.* **2022**, 1−1869.
(32) Khawal, H. A.; Gawai, U. P.; Asokan, K.; Dole, B. N. Modified Structural, Surface Morphological and Optical Studies of Li3+ Swift Heavy Ion Irradiation on Zinc Oxide Nanoparticles. *RSC Adv.* **2016**, *6*, 49068−49075.
(33) Islam, A.; Das, C.; Choudhury, S.; Mehnaz, S. Structural and Optical Characterization of Vacuum Evaporated Zinc Selenide Thin Films. *Eur. Sci. J.* **2014**, *10* ().
(34) Bindu, P.; Thomas, S. Estimation of Lattice Strain in ZnO Nanoparticles: X-Ray Peak Profile Analysis. *J. Theor. Appl. Phys.* **2014**, *8*, 123−134.
(35) Opanasyuk, A. S.; Kurbatov, D. I.; Ivashchenko, M. M.; Protsenko, I. Y.; Cheong, H. Properties of the Window Layers for the CZTSe and CZTS Based Solar Cells. *J. Nano-Electron Phys.* **2012**, *4*, 1−3.
(36) Nasiri-Tabrizi, B.; Fahami, A. Structural Characterization of Nanocrystalline Ni_(50-x)Ti<-Sub>50</Sub>Cu_X (X = 5, 9 Wt %) Alloys Produced by Mechanical Alloying. *Adv. Nanopart.* **2013**, *02*, 71−77.
(37) Rosli, A. N.; Zabidi, N. A.; Kassim, H. A. Ab Initio Calculation of Vibrational Frequencies of ZnSe and the Raman Spectra. *AIP Conf. Proc.* **2014**, *1588*, 265−270.
(38) Brus, L. E. Electron-Electron and Electron-Hole Interactions in Small Semiconductor Crystallites: The Size Dependence of the Lowest Excited Electronic State. *J. Chem. Phys.* **1984**, *80*, 4403−4409.
(39) Brus, L. E. A Simple Model for the Ionization Potential, Electron Affinity, and Aqueous Redox Potentials of Small Semiconductor Crystallites. *J. Chem. Phys.* **1983**, *79*, 5566−5571.
(40) Brus, L. Electronic Wave Functions in Semiconductor Clusters: Experiment and Theory. *J. Phys. Chem.* **1986**, *90*, 2555−2560.
(41) Shi, L.; Wang, C.; Wang, J.; Fang, Z.; Xing, H. Temperature-Dependent Raman Scattering of ZnSe Nanowires. *Adv. Mater. Phys. Chem.* **2016**, *06*, 305−317.
(42) Li, H.; Wang, B.; Li, L. Study on Raman Spectra of Zinc Selenide Nanopowders Synthesized by Hydrothermal Method. *J. Alloys Compd.* **2010**, *506*, 327−330.
(43) Lu, G.; An, H.; Chen, Y.; Huang, J.; Zhang, H.; Xiang, B.; Zhao, Q.; Yu, D.; Du, W. Temperature Dependence of Raman Scattering of ZnSe Nanoparticle Grown through Vapor Phase. *J. Cryst. Growth* **2005**, *274*, 530−535.
(44) Mohan, L.; Sisupalan, N.; Ponnusamy, K.; Sadagopalan, S. One Step Synthesis and Characterization of ZnO−ZnSe Heterostructures by Chemical Precipitation and Its Solar Photocatalytic Activity. *J. Inorg. Organomet. Polym. Mater.* **2020**, *30*, 2626−2632.
(45) Beena, V.; Ajitha, S.; Rayar, S. L.; Parvathiraja, C.; Kannan, K.; Palani, G. Enhanced Photocatalytic and Antibacterial Activities of ZnSe Nanoparticles. *J. Inorg. Organomet. Polym. Mater.* **2021**, *31*, 4390−4401.
(46) Beena, V.; Ajitha, S.; Rayar, S. L.; Ahmad, A.; Khan, M.; Abualnaja, K. M.; AlMasoud, N.; Ouladsmne, M. Photocatalytic Observation of Visible-Light-Driven Ag-Doped ZnSe Nanoparticles and Their Bio-Effectiveness. *Int. J. Environ. Sci. Technol.* **2022**, 10223.

https://doi.org/10.1021/acsomega.2c07654
ACS Omega 2023, 8, 13670−13679